Mechanical Systems and Signal Processing 184 (2023) 109652

Contents lists available at ScienceDirect

Mechanical Systems and Signal Processing

journal homepage: www.elsevier.com/locate/ymssp

Virtual pre-test analysis for optimization of multi-channel control strategies in direct field acoustic testing

A.G. de Miguel [a,*], M. Alvarez Blanco [a], E. Matas [a], H. Bériot [a], J. Cuenca [a], O. Atak [b], K. Janssens [a], B. Peeters [a]

[a] Siemens Industry Software NV, Interleuvenlaan 68, 3001 Leuven, Belgium
[b] Siemens Digital Industries Software, Francis House, 112 Hills Rd, Cambridge CB2 1PH, United Kingdom

ARTICLE INFO

Communicated by J.E. Mottershead

Keywords:
Direct field acoustic testing
Environmental testing
Digital Twin
MIMO control
Finite element modeling

ABSTRACT

Direct field acoustic excitation testing, or DFAX, is gaining the attention of the space industry as a reliable and flexible method to perform acoustic qualification tests of spacecrafts. The test aims at reproducing the sound conditions of the space launch using an array of high-powered loudspeakers placed around the test specimen. To achieve this end, advanced multi-input multi-output (MIMO) control strategies are employed to design the independent signals which drive the different speakers based on the responses acquired at the control locations over the test volume. Consequently, the performance and overall efficiency of the test campaign is then determined by a number of factors, among them stack configuration, test specimen orientation, number of speakers, control matrix and sensor location. To assist engineers in the design of such tests, this work proposes the use of numerical models to simulate the entire test set-up before the on-site campaign takes place. State-of-the-art vibro-acoustic solvers are employed to predict the pressure responses at all points in the test volume for various design choices, allowing test engineers to perform a virtual pre-test analysis based on numerical solutions to optimize their control strategy. The results included in this work illustrate the methodology followed to account for all the transfer functions of the electro-acoustic system as well as the validation of the levels of accuracy which can be achieved in a full-scale DFAX test via direct comparison with experimental measurements.

1. Introduction

In the space industry, environmental acoustic tests are performed to ensure that the spacecraft will safely reach its destination without failing due to the vibrations generated by the sound pressure levels reached during launch. The test specification aims at reproducing the acoustic levels at the interior of the launcher fairing, which are produced by different sources such as: turbulent boundary layer, separated flow, shocks, and lift-off environment [1]. In such scenario, the common assumption is that the sound field acting on the structure is diffuse [2], i.e. the field is homogeneous and isotropic and, therefore, there is no preferred direction of the sound.

Until recently, the standard approach to conduct such tests was in large reverberant chambers [3], which reproduce a diffuse sound field via overlapping of numerous room modes, as described by Cook et al. [4]. The reverberant room must be large enough to achieve a certain modal overlap at low frequencies [5], and, consequently, there are only a few of them worldwide which are suitable for spacecraft testing. Although in these chambers the diffuse sound field is well satisfied (above a certain frequency

* Corresponding author.
E-mail address: alberto.garcia_de_miguel@siemens.com (A.G. de Miguel).

https://doi.org/10.1016/j.ymssp.2022.109652
Received 20 December 2021; Received in revised form 29 June 2022; Accepted 4 August 2022
Available online 28 August 2022

threshold), the overall cost and risk of transporting the payload to such facilities are also important factors that cannot be neglected. Addressing these concerns, direct field acoustic excitation testing (DFAX) was introduced as an alternative method to conduct acoustic qualification tests that does not require a specific facility, but a large set of high-powered loudspeakers placed around the test specimen [6]. In this manner, the payload is excited by the sound waves coming directly from the loudspeakers without bouncing first in another surface. The main advantage of this approach is that the electro-acoustic set-up can be delivered and mounted anywhere, thus increasing the flexibility of the campaign schedule and decreasing drastically the risks associated with the shipment of the hardware to be tested. However, these advantages of DFAX are challenged by concerns about the levels of uniformity that can be achieved by direct fields, which might be compromised by the appearance of standing waves due to reflections from the spacecraft surfaces and the speaker stacks, as well as constructive and destructive interferences between the multiple speakers. It has been demonstrated that these effects can be mitigated by selecting a proper control system, as shown for instance by Larkin [7], and, consequently, vast efforts have been invested in the past years in the implementation of advanced multi-channel strategies to achieve more reliable and safer tests.

Single-input single-output (SISO) control strategies have proven to perform poorly in DFAX due to the large sound pressure level (SPL) variations generated when a single signal is employed to drive all the loudspeakers, while multiple-input multiple-output (MIMO) strategies offer a superior capability to control the wave interferences in the test volume [6]. The reason is that the use of multiple signals to drive groups of speakers avoids fully correlated sound fields, and the availability of various control sensors allows for the explicit specification of the spatial correlation properties in the target matrix. The performance of the control system, and thus the test, is defined by different factors such as the conditioning of the frequency response matrix of the system or the capability of the electro-acoustic plant to realize the spatial correlation properties of the target matrix. In order to improve the latter, a pre-test analysis was recently introduced [8] to automatically define key parameters in MIMO random control tests based on an experimental model of the plant derived from the identification of the system responses. The method, which is already being used in qualification tests of space hardware via DFAX, see for instance [9], has proven useful in reducing the dynamic range of the measured pressures at the microphones, while avoiding time-consuming trial and error iterations in the search for an optimal set of control sensors.

Due to the aforementioned challenges in DFAX, the NASA handbook [1] recommends to perform comprehensive analyses of the acoustic field and structural response, although it admits the difficulty of doing such analyses with MIMO control strategies. Indeed, if the responses of the control system are to be predicted with a certain degree of accuracy, the simulation must include all the signal transformations of the electro-acoustic plant. Similar virtual testing approaches have been recently introduced in different fields, such as aircraft [10], spacecraft [11] or automotive [12]. These Digital Twins aim at substituting the physical set-up with comprehensive simulations to avoid building expensive prototypes to qualify the system as well as testing at the component level. In space applications, these refined models were also used for pre-test and post-test [13] analyses, as well as to improve the level of numerical–experimental correlation for coupled load analysis [3,14]. In vibration tests, the environmental factors and boundary conditions play a significant role in the responses measured at the sensors. To meet these challenges, a set of virtual shaker techniques have been recently introduced to account for the dynamics of the test facility (control, power amplification, shaker dynamics and test specimen) leading to a high-fidelity representation of the control test [15].

These philosophies were introduced in the context of DFAX by Alvarez Blanco et al. [16,17] to study the performance of the MIMO controller. The experience showed that, in acoustic tests, the boundary conditions, e.g. cross-over filters, loudspeaker performance or wave interferences with the set-up, can also have a large effect on the system response. It became clear that, in order to use such Digital Twin of the DFAX system in engineering applications, the MIMO control strategy and the dynamics of all its sub-systems must be included in the simulation to enable accurate estimation of the quantities measured in physical tests. Aiming at that, previous works [18,19] showed that the loudspeaker performance can be well represented by accounting for the electro-mechanic transformation between the input signals and the mechanical movement of the membranes. In this work, a comprehensive model of the DFAX set-up in [16] is generated, applied as a tool for the design of the test layout and control parameters, and validated against experimental data of a full DFAX. The comprehensive simulation aims at predicting with high levels of accuracy the most relevant responses in the electro-acoustic plant, including the digital audio processing, the loudspeakers performance, the acoustic wave propagation and the payload couplings. In particular, the electro-dynamic models of the direct radiators are based on the lumped parameter models of Beranek and Mellow [20] and the geometric layout is represented via a finite element model (FEM) of the full loudspeaker set-up and payload. Due to the large volume to be analyzed for a typical DFAX test, a state-of-the-art adaptive order FEM model introduced by Bériot et al. [21], also known as FEMAO, is utilized to solve the acoustic problem in the frequency domain. The acoustic model assumes free-field conditions [22] and is strongly coupled with the payload model to account for the vibro-acoustic interactions in both ways.

By using the proposed Digital Twin in the early stages of the test planning, engineers can perform all the design iterations of the layout in the computer, thus reducing the overall time of the test campaign. Furthermore, the availability of full-field solutions provided by the numerical model enables the evaluation of the system responses at any point, not only at a reduced amount of sensors, consequently reducing the risks on the payload when conducting the physical test. To illustrate the capabilities of the proposed approach, and inspired by the experimental pre-test analysis in MIMO random control tests, this work introduces a simulation-based pre-test in which the system identification is substituted by the frequency responses generated by the virtual model. The results show how this approach, hereinafter referred as virtual pre-test analysis, can be used to improve the selection of the control sensors for any given electro-acoustic layout. Then, the Digital Twin enables the prediction of the responses produced by any chosen control strategy with full-field confidence, even before the physical set-up has been installed. The current work also

represents the first building block of a true Digital Twin that can be updated onsite once the electro-acoustic plant is ready, and used for online predictions in DFAX tests. Such capabilities will be shown in subsequent works.

The paper is organized as follows: first, Section 2 introduces the basic theoretical aspects of MIMO random control and pre-test analysis. The proposed Digital Twin is discussed in Section 3, which includes a description of all the components analyzed as well as the introduction of the virtual pre-test approach. The results are included in Section 4. These include a correlation simulation/experiment using references from a DFAX test performed in 2017 in the facilities of Thales Alenia Space in Toulouse (Section 4.1), the validation of the virtual pre-test analysis via comparison with synthesized references from the same test (Section 4.3) and the application of the proposed approach using full-field data (Section 4.4). Finally, the conclusions of the work are drawn in Section 5.

2. Control strategy

The main function of the controller in a DFAX test is to design the set of signals driving the loudspeakers, aiming at reproducing the properties of the sound fields defined as target reference. In space applications, these references are expressed as a spectrum of uniform SPL, typically defined in one-third octave bands [23]. Closed-loop random control systems are employed to recreate broadband random acoustic environments, which are generated by a carefully designed combination of loudspeaker systems with different frequency ranges. As introduced in Section 1, MIMO control strategies offer a superior performance in achieving the required level of uniformity in the sound field, therefore they have become the standard in DFAX tests.

2.1. MIMO control

In a MIMO scenario, the dynamics of the control system are characterized by its frequency response matrix, $\boldsymbol{H}(\omega) \in \mathbb{C}^{L\times M}$, which contains the frequency response functions (FRF) between input signals, M, and output responses, L. The latter corresponds to the readings at the acoustic sensors placed in the DFAX volume, i.e. L is equal to the number of control microphones. It is here assumed that the system is linear and time-invariant, thus all the formulas are expressed in frequency domain. For the sake of simplicity, the dependency with respect to the angular frequency, ω, is omitted hereinafter.

The correlation properties of the desired acoustic field are defined through a spectral density matrix (SDM),

$$\boldsymbol{S}_{\boldsymbol{dd}} = E[\boldsymbol{p}_{\boldsymbol{d}}\boldsymbol{p}_{\boldsymbol{d}}^{H}], \tag{1}$$

where $\boldsymbol{p}_{\boldsymbol{d}} \in \mathbb{C}^{L\times 1}$ is a vector containing the Fourier transforms of the desired pressure responses at the output sensors, E is the expectation operator and H indicates Hermitian transpose. $\boldsymbol{S}_{\boldsymbol{dd}}$ contains then the power spectral densities (PSD) in the diagonal elements and the cross-power spectral densities (CSD) in the out-of-diagonal elements. On the other hand, the statistical properties of the drive signals can be represented by the input SDM:

$$\boldsymbol{S}_{\boldsymbol{xx}} = E[\boldsymbol{x}\boldsymbol{x}^{H}], \tag{2}$$

where $\boldsymbol{x} \in \mathbb{C}^{M\times 1}$ is the vector containing the signals spectrum. The output spectra at the microphone sensors is related to the signal inputs through the frequency response matrix, as follows:

$$\boldsymbol{p} = \boldsymbol{H}\boldsymbol{x}, \tag{3}$$

which leads to the expression to obtain the output SDM:

$$\boldsymbol{S}_{\boldsymbol{pp}} = \boldsymbol{H}\boldsymbol{S}_{\boldsymbol{xx}}\boldsymbol{H}^{H}, \tag{4}$$

where $\boldsymbol{S}_{\boldsymbol{pp}} \in \mathbb{C}^{L\times L}$. The objective of the MIMO control algorithm is to obtain a $\boldsymbol{S}_{\boldsymbol{pp}}$ matrix that is statistically equivalent to $\boldsymbol{S}_{\boldsymbol{dd}}$ of Eq. (1). To achieve that, the controller designs a set of optimal signals that minimize the error between the two spectral matrices. This problem can be solved in a least-squares sense via the pseudo-inverse of the matrix of plant responses [24,25], as follows:

$$\boldsymbol{S}_{\boldsymbol{uu}} = \boldsymbol{H}^{\dagger}\boldsymbol{S}_{\boldsymbol{dd}}(\boldsymbol{H}^{\dagger})^{H}, \tag{5}$$

where $\boldsymbol{S}_{\boldsymbol{uu}} \in \mathbb{C}^{M\times M}$ is the SDM of the optimal drive spectra, $\boldsymbol{u}$. The symbol † refers to the pseudo-inverse operator.

By combining Eqs. (4) and (5), and defining $\boldsymbol{S}_{\boldsymbol{uu}} = \boldsymbol{S}_{\boldsymbol{xx}}$, the resulting output responses of the closed loop can be estimated as

$$\boldsymbol{S}_{\boldsymbol{pp}} = \boldsymbol{H}\boldsymbol{H}^{\dagger}\boldsymbol{S}_{\boldsymbol{dd}}(\boldsymbol{H}\boldsymbol{H}^{\dagger})^{H}. \tag{6}$$

The capability of the controller to achieve the desired field responses depends on the dynamics of the electro-acoustic plant. In the current formulation, these factors reflect on the properties of the frequency response matrix, $\boldsymbol{H}$, as well as on the conditioning of the problem. A detailed description of this topic is out of the scope of this work and the reader is referred to [8,24] if interested.

2.2. Pre-test analysis

The test specification, expressed in one-third octaves, represents the maximum acoustic level expected at each frequency band inside the launcher's payload bay, and does not include any information regarding the correlation properties of the acoustic

fields, which are assumed to be diffuse in operation. In order to generate a realizable $\boldsymbol{S}_{\boldsymbol{dd}}$ matrix for MIMO random control, a pre-test analysis step was recently proposed [8] as a mean to improve the control strategy via two steps: the unconstrained projection algorithm (UPA) and the optimization search, which are briefly described in the following. For more details about the implementation of these processes, the reader is referred to [8,16].

A requirement to perform the pre-test analysis is that the quantity of available sensors, T, should be greater than the desired number of control sensors, L. This leaves a certain amount of sensors which are used for monitoring purposes. The analysis is based on the use of a non-parametric model of the electro-acoustic system, which is generated from the system identification step[1] and represented by the frequency response matrix $\boldsymbol{H}^{\boldsymbol{t}} \in \mathbb{C}^{T\times M}$. Note that since in acoustic tests the noise is mainly expected at the outputs, the H1 estimator is employed to obtain this matrix.

The UPA is an iterative procedure that aims at improving the realizability of target matrix, $\boldsymbol{S}^{\boldsymbol{t}}_{\boldsymbol{dd}} \in \mathbb{C}^{T\times T}$, for a fixed MIMO control system. The algorithm search the convergence of the diagonal elements towards the test specification, adding no constrains in the definition of the out-of-diagonal elements which define the spatial correlation of the sound field. This means that, based on the test specification, the sound uniformity is always enforced but the coherence values and phases might not match those of a diffuse field.

On the other hand, the optimization algorithm focuses on the automatic selection of an optimal set of control microphones, L, among the available set, T, based on the comparison of the predicted responses with the test specification. An exhaustive search is performed to evaluate all possible combinations without repetition of L within T, hereinafter referred to as *candidates*. It is noted that, for practical reasons, a maximum value can be defined to stop the optimization loop. The chosen criteria to discard sub-optimal candidates is based on two metrics:

- Number of bands out of tolerance: amount of SPL responses in all T sensors which exceed the tolerances specified in the test targets, e.g. −1/+3 dB at a certain one-third octave band.
- Root mean squared error (RMSE): deviation of the spatial average of SPL from the specification.

In general, the candidates are ordered on the basis of the first of these metrics, from minimum to maximum number of bands out of tolerance. Then, the RMSE is utilized to discern between candidates with equal value of the first metric. As a result of the pre-test, the user can make a data-driven decision when it comes to selecting the control sensors using the predictions of SPL uniformity and power requirements of each candidate.

3. Digital twin

The aim of the present work is to introduce a Digital Twin of the DFAX system that substitutes the role of the experimental non-parametric model obtained in the system identification stage of the test campaign. In order to achieve that, it was paramount to derive a series of simulation models that represent with a sufficient degree of accuracy the electro-vibro-acoustic phenomena involved in this type of acoustic tests. Each of these models simulates the behavior of a different component of the system, accounting for the transformations of the signals from the control system to the acoustic responses measured at the microphones. The proposed applications of such an approach extend beyond the classical use of simulation tools for test design, such as what-if scenarios and design optimizations. Indeed, a virtual pre-test analysis is presented here based on the use of the simulated transfer functions of the electro-acoustic plant in the framework described in Section 2.2.

The Digital Twin is composed of three models that represent the digital audio processing, the electro-dynamic transducers and the sound transmission in the test volume. Fig. 1 shows a diagram of the different modeling blocks included in the simulation framework and the connections between them. It also gives an idea of the signal flow between the signal generator and the sensors in a DFAX system. The labels shown in the diagram are described throughout this section. It is assumed that the system is time invariant and linear, i.e. its properties remain unchanged over time and with respect to any external or internal parameter. As a consequence of the former hypotheses, all the variables modeled in this framework are described as frequency responses.

3.1. Signal processing

The digital audio processing unit transforms and distributes the input signals to the different speaker units. In general, it can be divided into the DSP, which provides equalization, delay and cross-over filtering capabilities, and the power amplifiers, that increase the signal level to that required by the electro-dynamic transducers. One way to represent the signal distribution is through the drive matrix, which defines the connectivity between the different input signals to the loudspeaker cabinets. This matrix can be written as

$$\boldsymbol{x}_{\boldsymbol{c}} = \boldsymbol{D}\, \boldsymbol{x}_{\boldsymbol{d}}, \tag{7}$$

where $\boldsymbol{x}_{\boldsymbol{d}} \in \mathbb{C}^{n_d\times 1}$ is a vector containing the Fourier transforms of the drive signals, with length is equal to the number of drives, n_d, and $\boldsymbol{x}_{\boldsymbol{c}} \in \mathbb{C}^{n_c\times 1}$ is a vector containing the electrical signals distributed to the different speaker cabinets. Note that $n_c \geq n_d$, i.e. the electro-acoustic plant will have at least a number of speaker cabinets equal to the number of input signals. Finally, the drive matrix, $\boldsymbol{D} \in \mathbb{Z}^{n_c\times n_d}$, is filled with ones or zeros based on the selected connections.

[1] In MIMO random control, the system identification is a procedure performed before the actual test to estimate the frequency responses of the plant. In general, these functions are obtained by means of a low-level open-loop test using random input signals.

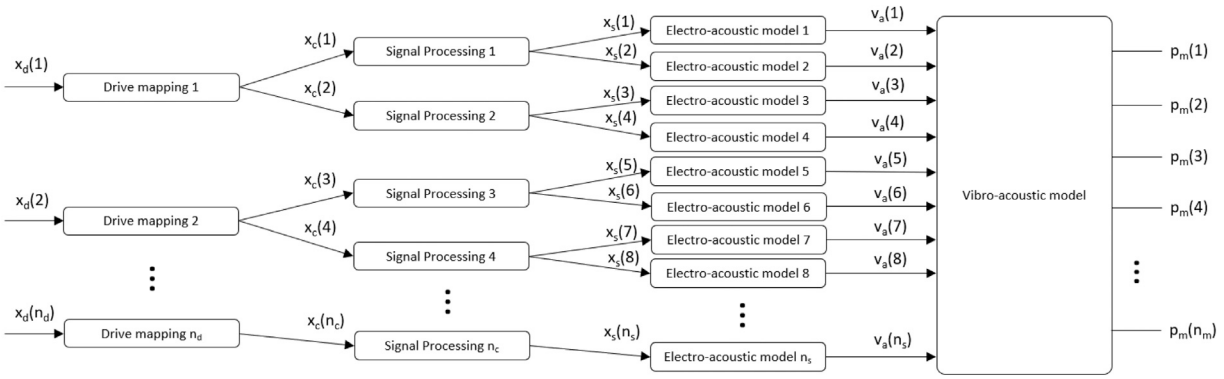

Fig. 1. Block diagram showing the models of all the signal transformation included in the Digital Twin the DFAX electro-acoustic plant.

High-powered loudspeakers as those typically used for DFAX usually contain different driver units to deliver proper sound levels at different frequency ranges, e.g. subwoofers, woofers and high-frequency drivers. The signal gains for each drive are then defined by the cross-over settings, which ensure certain performance of the sound system in overlap regions in the frequency spectrum. The signal amplification in the whole electro-acoustic plant can be written as follows:

$$\boldsymbol{x_s} = \boldsymbol{A}\,\boldsymbol{x_c}, \tag{8}$$

where $\boldsymbol{x_s} \in \mathbb{C}^{n_s \times 1}$ contains the spectrum of the voltage inputs at each speaker driver, being n_s the total number of drivers. The amplification matrix $\boldsymbol{A} \in \mathbb{C}^{n_s \times n_c}$ contains all the cross-over functions over the targeted frequency range. For clarity purposes, an example of this matrix is included here:

$$\boldsymbol{A} = \begin{bmatrix} A_1 & A_2 & A_3 & 0 & 0 & 0 & 0 & 0 & 0 & 0 & 0 & 0 \\ 0 & 0 & 0 & A_1 & A_2 & A_3 & 0 & 0 & 0 & 0 & 0 & 0 \\ 0 & 0 & 0 & 0 & 0 & 0 & A_1 & A_2 & A_3 & 0 & 0 & 0 \\ 0 & 0 & 0 & 0 & 0 & 0 & 0 & 0 & 0 & A_1 & A_2 & A_3 \end{bmatrix}^T \tag{9}$$

which represents a system with $n_c = 4$ cabinets and $n_s = 12$ speaker drivers of 3 different types. A_1, A_2 and A_3 are the amplification gains of each driver defined by the cross-over settings.

In this research, two types of loudspeaker cabinets were analyzed: a subwoofer featuring two large drivers and a three-way cabinet embedding a pair of woofers, mid-range drivers and tweeters. Due to the availability of test data of the amplification functions, an experimental model of the frequency response of the power amplifications are utilized in this work. Fig. 2 shows the gain curves over the frequency of the three aforementioned drivers, which illustrates the effects of the cross-over filters for different drivers (subwoofer, woofer and mid-range driver).

Finally, by combining Eqs. (7) and (8) one can obtain the total frequency response matrix of the digital audio processing system as:

$$\boldsymbol{H_{el}} = \boldsymbol{A}\,\boldsymbol{D}, \tag{10}$$

whose dimensions are $n_s \times n_d$. This matrix provides the relation between the input voltage seen by each speaker unit and the drive signals sent by the control system.

3.2. Electro-acoustic model

The transformation of the electric signals into acoustic energy is performed by the electro-acoustic transducers, usually referred to as loudspeakers. These devices exploit the dynamic response of a voice-coil system to excite the unidirectional movement of a membrane structure, which delivers energy to the surrounding air in the form of acoustic waves. In the context of DFAX, the frequency response matrix of the full electro-acoustic plant containing n_s speakers can be expressed as:

$$\boldsymbol{v_a} = \boldsymbol{H_{ea}}\,\boldsymbol{x_s}, \tag{11}$$

where $\boldsymbol{v_a} \in \mathbb{C}^{n_s \times 1}$ represent the acoustic velocities radiated into the test volume by all the speaker drivers, and $\boldsymbol{H_{ea}} \in \mathbb{C}^{n_s \times n_s}$ is the frequency response matrix expressing the conversion between electrical and acoustic energies. It is noted that, in this format, $\boldsymbol{H_{ea}}$ is a diagonal matrix and thus can be rewritten as:

$$\boldsymbol{H_{ea}} = diag(\boldsymbol{f}), \tag{12}$$

where the vector $\boldsymbol{f} \in \mathbb{C}^{1 \times n_s}$ contains the electro-acoustic transfer functions of the drivers, i.e. $\boldsymbol{f} = \{f_1 \;\; f_2 \;\; f_3 \;\; \ldots \;\; n_s\}$ and the operator $diag$ transforms the vector $\boldsymbol{f}$ into a diagonal matrix. In general, it is fair to assume that the electro-dynamic transducers of the same type will produce a very similar response, thus $\boldsymbol{f}$ will contain repeated functions and could be further simplified.

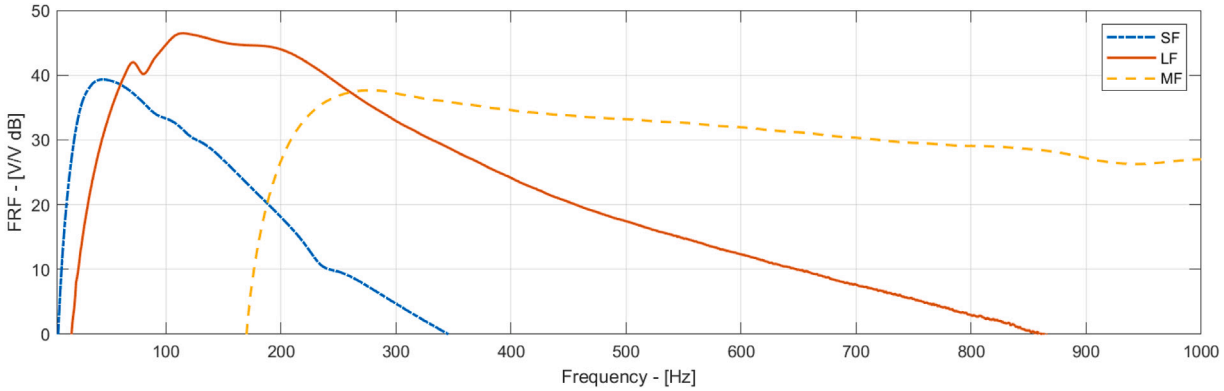

Fig. 2. Amplification gains measured at three different drives used in DFAX: subwoofer (SF), woofer (LF) and mid-range driver (MF).

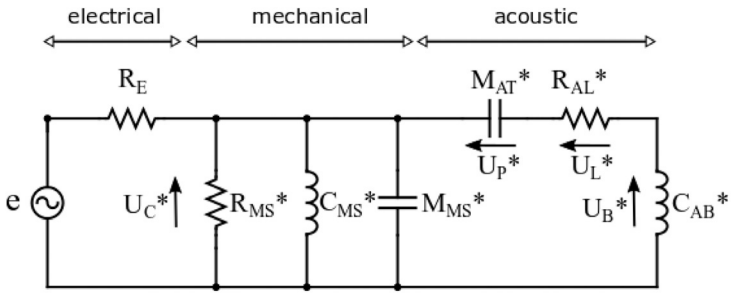

Fig. 3. Equivalent electro-acoustic circuit of a vented-box loudspeaker referred to the electrical side.
Source: Reproduced from [20].

Different modeling approaches are available in the literature to model in detail the electro-acoustic response of loudspeakers. These are usually based on the use of FEM to represent the geometry of the different components of the system as in [26,27], or in combinations of FEM/BEM to model the acoustic cavity and surroundings [28,29]. However, the overall size and complexity of the DFAX electro-acoustic plant, together with the lack of available data of the detailed design of the loudspeaker components, is such that the use of highly detailed numerical models would increase considerably the modeling effort. For this reason, simplified models based on analytical functions are utilized whenever possible. For direct radiators, such as sub-woofers and woofers, lumped parameter models are a widely spread tool to describe the behavior of the loudspeaker based on a reduced set of constants, a.k.a. Thiele–Small parameters [30,31]. An example of the equivalent circuit for a vented-box loudspeaker derived in [20] and utilized in this work is displayed in Fig. 3. Based on this representation, the loudspeaker is characterized by the following parameters: electrical voice coil resistance (Re), mechanical losses factor (Q_{ms}), electrical losses factor (Q_{es}), equivalent air volume of suspension (V_{as}), driver resonance frequency (f_s) and diaphragm area (S_d). Also, some extra details regarding the enclosure and vent dimensions must be provided to properly include the back cavity effect and port contributions.

The frequency response obtained from the model of Fig. 3 applied to one of the woofers used in this research is included in Fig. 4. The plot shows a comparison of the FRF (diaphragm velocity over voltage input) derived from the model against experimental data. The latter was obtained from measurements taken with a Laser Doppler Velocimetry (LDV) system pointing at the center of the speaker's membrane, see [18,19] for more details on loudspeaker characterization. One can observe that the model captures fairly well the overall response of the transducer, including the resonance frequency of the vent (corresponding to the main dip at approx. 60 Hz). An underestimation of the membrane velocity is observed at frequencies above 100 Hz, which is most likely due to uncertainties in the Thiele–Small parameters. It is important to point out that these results were obtained using the nominal parameters provided by the manufacturer for the single driver, thus certain offsets are expected with respect to the operational response when installed in the loudspeaker cabinet. The accuracy of the loudspeaker model could be further improved via parameter optimization techniques, if needed. It is also noted that the response shown in Fig. 4 does not include the contribution of the port radiation, which is dominant around the resonance frequency.

The introduction of proper models to represent the response of the electro-acoustic transducers is a crucial part of the Digital Twin. In general, any model providing the transfer functions between the input voltage and the acoustic velocity can be used in the proposed framework. For instance, an experimental model was employed in this research to represent the more complex response of the mid-range driver, which consist of a horn-driver system. Also, the assumption in this work is that all the sub-systems behave linearly, thus the loudspeaker responses are equal at small and high amplitudes. In reality, there are certain effects that can cause a non-linear response of the drivers, such as heating of the coil, non-linear stiffness of the suspension and break-up modes

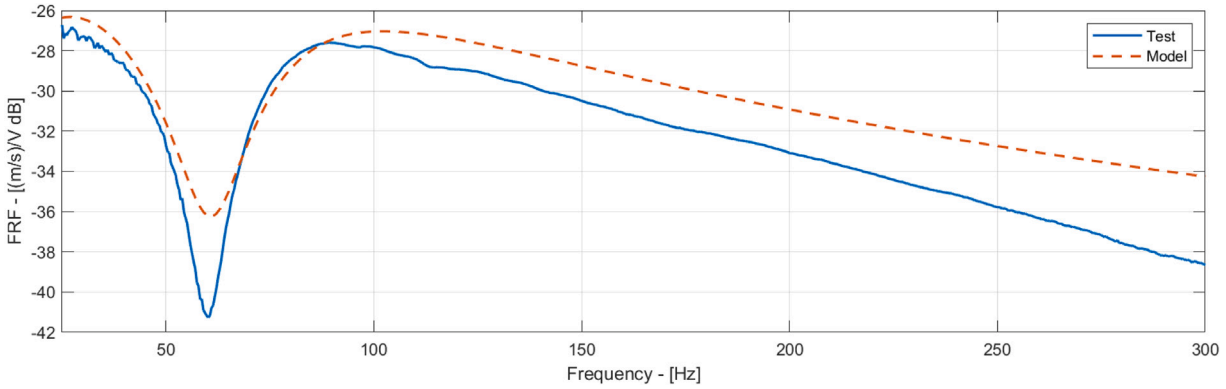

Fig. 4. Comparison of the frequency response measured (Test) and simulated (Model) for the woofer. The cross-over frequencies for this driver were 80 Hz (high-pass) and 250 Hz (low-pass).

of the membrane, among others [32]. Further studies must be conducted to evaluate the introduction of such effects in the current framework.

3.3. Vibro-acoustic FEM model

The complex layout of DFAX calls for the use of advanced simulation models to predict the pressure fields in the test volume. Indeed, the acoustic responses do not only depend on the direct radiation from the speakers, but also on the wave reflections off the speaker stacks and the test specimen. As a consequence, a deterministic numerical approach such as the finite element method is deemed the most suitable strategy for this application, thanks to its ability to model all the geometrical features of the electro-acoustic plant in detail. The ultimate goal of the acoustic model is to provide the relation between the acoustic loads, which are provided by the electro-acoustic models introduced in Section 3.2, and the pressure measured at the microphones points over the test volume. This relation can be written as

$$\boldsymbol{p_m} = \boldsymbol{H_{ac}}\, \boldsymbol{v_a} \tag{13}$$

where $\boldsymbol{p_m} \in \mathbb{C}^{n_m \times 1}$ contains the vector of pressure responses at all the virtual microphones, n_m.

As mentioned earlier, due to the presence of a large volume, the acoustic propagation, modeled by the Helmholtz equation, requires an efficient approach. In this work, a high-order hierarchical p-FEM approach is employed. The use of high-order FEM is motivated by the fact that it has shown to provide massive reductions in both memory and CPU time compared to classical finite-element models, and even superior performance to state-of-the-art Trefftz approaches on a series of Helmholtz problems (see e.g. [33,34]). In order to further maximize computational efficiency, an adaptive strategy, introduced by Bériot et al. [21], and which relies on a single coarse mesh is adopted. In this approach, an a-priori error indicator is used to adjust the order automatically in the elements so as to maintain a target accuracy. In practice, the order ranging from $p \in [1, 10]$ is adjusted locally, prior to each calculation, based on the element size, distortion and frequency so as to reach a user defined target accuracy E_t while minimizing the cost [35]. In this study, all computations were performed using a typical engineering target accuracy of $E_t = 5\%$. The structure of the specimen on the other hand, is discretized using a conventional isoparametric linear dynamics formulation, with physical variables. Note that in case of larger structures, a modal representation may also be leveraged to alleviate the computational burden of the coupled analysis.

Let us now describe step by step the 3D vibro-acoustic model creation process. To ease the model preparation, minimize modeling errors, and maximize computational efficiency, this process is streamlined and almost fully automated. The structural mesh of the component under test, which is assumed to be a prerequisite of the proposed DFAX approach, is first imported. In parallel, a surface mesh of the loudspeaker cabinets and membranes is created, using a user defined characteristic length. An approximate convex hull is then automatically computed, by applying the quickhull algorithm [36] on a random selection of points on all surfaces (including ground). To create the exterior surface of the computational domain, this convex hull is then scaled in the exterior normal direction, and a typical "bell shape", enclosing the cabinet and specimen is obtained (see Fig. 5). The latter is homogeneously triangulated and the test volume, which is defined as the difference between the bell shape volume and the union of the specimen and cabinets, is then discretized using a conventional filler algorithm, typically employing 4-noded linear tetrahedral elements. A strong vibro-acoustic coupling approach is adopted here, meaning that the frequency response of the structural and acoustic models are solved together at once, in physical coordinates. Although more challenging, this approach is preferred as it allows to account for the complex interactions at play between the specimen structures and the direct acoustic field in the volume. It is worth noting that on the vibro-acoustic interface, the structural and acoustic surfaces are typically not matching, not only in terms of grid size (the acoustic mesh size being typically an order of magnitude larger than the structural one) but also in terms of element order (the acoustic

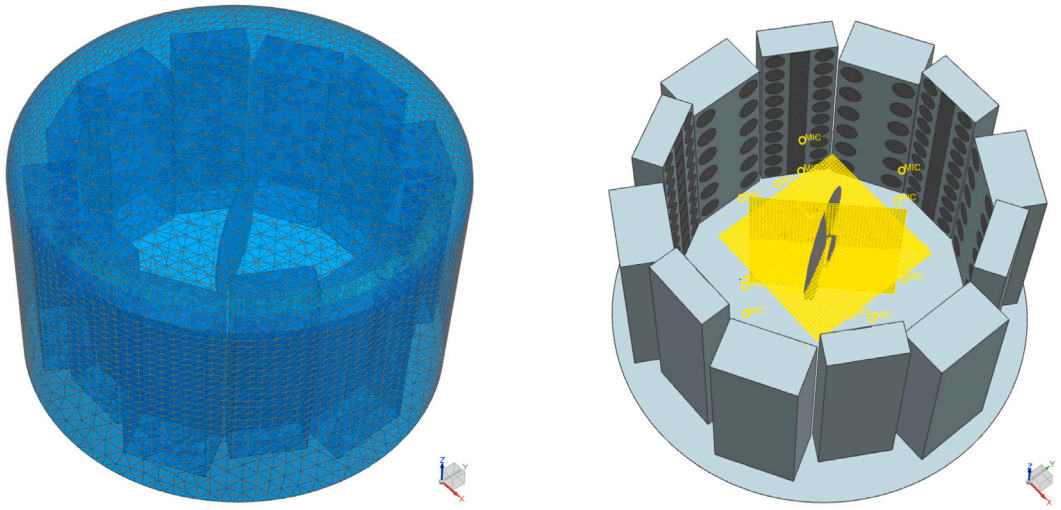

(a) (b)

Fig. 5. Numerical model in Simcenter 3D: acoustic mesh (a) and geometry with structural model and microphone sensors (b). FEM model of the antenna courtesy of Thales Alenia Space.

pressure being discretized with higher-order polynomials). This requires a dedicated approach to accurately compute the coupling fluxes, and a common refinement strategy is adopted here.

In terms of boundary conditions, the ground is assumed to be acoustically rigid and an acoustic absorption coefficient is applied on the cabinet walls to add some damping to the system. As the actual impedance of the speaker cabinets was not known, an overall value of 0.2 was utilized for the absorption coefficient. This value was based on correlation analyses performed previously for similar models. A load is prescribed on the loudspeaker membranes, under the form of a prescribed panel velocity boundary condition. On the exterior bell-shape surface, a locally-conformal implementation of the Perfectly Matched Layer (PML), referred to as the Automatically Matched Layer (AML) described in [22], is used in order to efficiently absorb the outgoing waves. In the AML approach, the absorbing region and its properties (number of layers and stretching function) are automatically generated in the solver.

The factorization of the resulting complex symmetric sparse matrix is performed using the MUMPS library version 5.0.1 [37], and frequency parallelism is leveraged to further accelerate the frequency sweep. Note that the computational cost of the coupled vibro-acoustic simulation is strongly frequency-dependent, owing to the automated p-adaptive nature of the acoustic model. Lower frequencies are less memory and cost intensive, whereas at higher frequencies, higher polynomial orders will be triggered in the cavity, see [21] for more details on the expected complexity.

3.4. Virtual pre-test

The proposed Digital Twin of the DFAX plant is composed of the three models previously introduced. In this manner, the main signal transformations in the MIMO test are properly described and any potential model uncertainties can be studied at the component level via correlation approaches. The overall transfer functions of the electro-acoustic plant are obtained by combining Eqs. (10), (11) and (13), as follows:

$$\boldsymbol{p_m} = \boldsymbol{H}_{sim}\, \boldsymbol{x_d} \tag{14}$$

where

$$\boldsymbol{H}_{sim} = \boldsymbol{H}_{ac}\, \boldsymbol{H}_{ea}\, \boldsymbol{H}_{el}. \tag{15}$$

$\boldsymbol{H}_{sim} \in \mathbb{C}^{n_m \times n_d}$ provides the transfer functions between the virtual sensors, n_m, and the drive signals, n_d. The generation of this matrix enables one to conduct a virtual pre-test analysis by only substituting the experimental system matrix, $\boldsymbol{H}$, by the virtual one, $\boldsymbol{H}_{sim}$. In this manner, the values of the initial drive signals can be predicted for a given acoustic reference, $\boldsymbol{S}^*_{dd}$, as

$$\boldsymbol{S}^*_{xx} = \boldsymbol{H}^{c}_{sim}{}^{\dagger}\, \boldsymbol{S}^*_{dd} (\boldsymbol{H}^{c}_{sim}{}^{\dagger})^H, \tag{16}$$

where the upper-script $*$ refers to simulation-based SDM arrays. In this expression, $\boldsymbol{H}^{c}_{sim}$ is a subset of $\boldsymbol{H}_{sim}$ containing the transfer functions at the control microphones. On the other hand, the pressure responses at all virtual sensors can be predicted as

$$\boldsymbol{S}^*_{pp} = \boldsymbol{H}_{sim} \boldsymbol{S}^*_{xx} \boldsymbol{H}^H_{sim}, \tag{17}$$

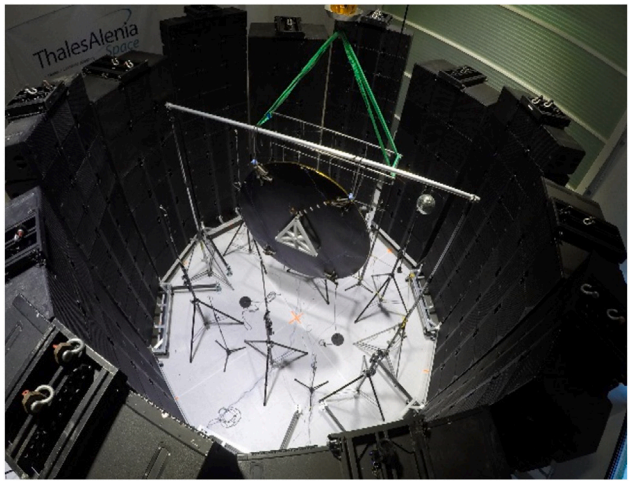

Fig. 6. Picture of the test set-up with the antenna reflector positioned in the center. Image courtesy of Thales Alenia Space.

where $\boldsymbol{S}_{pp}^{*} \in C^{n_m \times n_m}$ contains the PSD and CSD predicted by the simulation model. On the basis of this formulation, the pre-test algorithms described in Section 2.2 can now be performed in a full virtual scenario including both the UPA and optimization algorithms.

The introduction of a virtual pre-test analysis extends the more traditional use of simulation models for test preparation by adding the control concerns already at the beginning stage of the campaign planning. Such approach has the potential to make the testing process more efficient through the a priori prediction of the MIMO control system performance, which can reduce the amount of timely onsite iterations to tune the control parameters. Moreover, engineers can exploit the full-field capabilities of the Digital Twin to perform an automatic selection of the control sensors based on simulation data, as it is demonstrated in the next section.

4. Results

The aim of this section is twofold: first, to validate the proposed models for the prediction of the system responses at the physical sensors; and secondly, to demonstrate the advantages of the use of full-field data in the design of the test layout and control strategy. The data used in this exercise as reference corresponds to a DFAX experiment carried out by Thales Alenia Space and Siemens in 2017, in which a composite antenna reflector of approx. 2 m of diameter was tested [38]. Fig. 6 displays a photograph taken at the test facility showing the electro-acoustic setup with the test specimen placed in the center. A total of 96 loudspeaker cabinets of two types were installed: 36 large sub-woofers and 60 3-way cabinets capable of exciting the structure beyond 10 kHz. The two cabinet models were stacked in 6 columns following a cylindrical pattern of inner radius equal to 2.615 m. The MIMO control system included 6 drive signals (here labeled as Drive1 to Drive6) and 30 microphones, among which 21 are analyzed in this work (here labeled as Mic1 to Mic21). The test was performed using a Simcenter SCADAS data acquisition system and the software Simcenter Testlab MIMO Random Control.

The numerical model was generated in Simcenter 3D based on the models described in Section 3 and it is illustrated in Fig. 5. The acoustic velocities obtained using the models in Sections 3.1 and 3.2 for the DSP settings and loudspeaker models, respectively, used in the test were introduced as boundary conditions in the FEMAO simulation. The frequency response analysis was solved from 21.875 to 1000 Hz, with a resolution of 3.125 Hz. The acoustic volume had an external radius of 3.8 m and a maximum height of 4.63 m, and was meshed with a total of 36,077 tetrahedral elements of adaptive order. At the maximum frequency (1000 Hz), the maximum element order in the analysis was 10, which was applied to 0.08% of the elements, whereas the most used order was 7, used in 28.46% of the elements. The structural model of the antenna, kindly provided by Thales Alenia Space, was modeled in free-free condition and linked to the acoustic mesh via two-way coupling, as depicted in Section 3.3. The size of the structural model was approx. 300,000 degrees of freedom, whereas that of the acoustic model ranged from circa 18,000 at 20 Hz to 1.7 M at 1000 Hz. All computations were performed on a fat node empowered with 2x Intel Xeon Gold 6246R CPU (16 cores each) with 1.5 Tera Bytes of RAM, using 16 parallel processes and lasting a total time of 1 h and 16 min.

The results are presented as follows: first, the frequency responses obtained from the Digital Twin are directly compared to those from the test references. Subsequently, the propagation of uncertainties in the MIMO problem is studied following a statistical approach. Then, a virtual pre-test analysis is performed using the computed transfer matrix and the procedure described in Section 3.4, and the predicted system responses are compared with those from experimental data. Finally, the full potential of the Digital Twin for pre-test is illustrated by showing the advantages of utilizing full-field responses to choose the control set and to de-risk the MIMO test. In the following results only pressure values are presented and discussed, however it is pointed out that the proposed method also provides the vibro-acoustic response of the test specimen. The validation of the simulated structural responses will be addressed in future works.

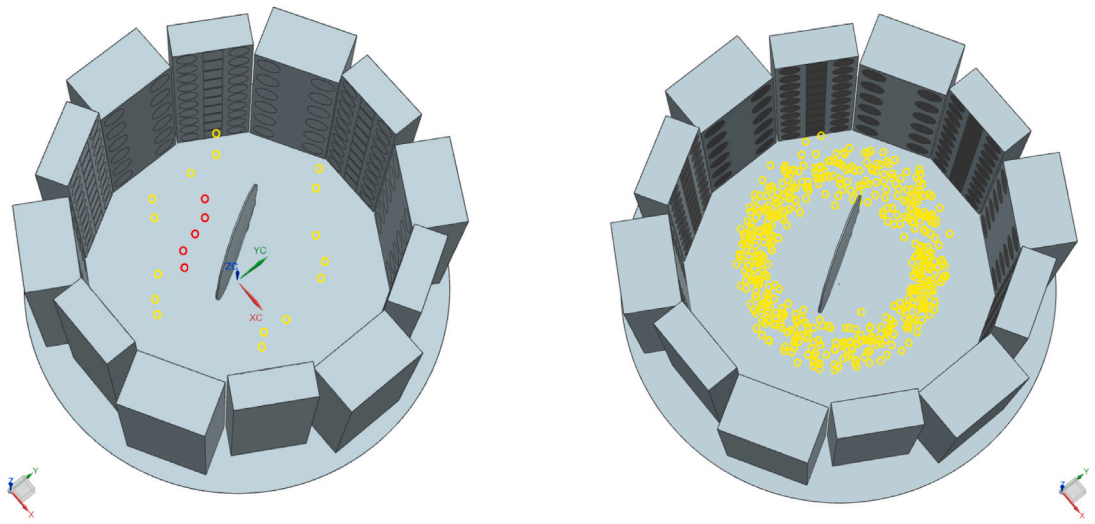

Fig. 7. Location of the physical sensors in the test (a) and the virtual sensors for full-field analysis (b).

4.1. Model validation

Fig. 7(a) shows a picture of the model with the microphones nodes placed in correspondence to the location of the physical sensors in the actual test. In the image, the yellow circles are the sensors that can potentially be used for control (Mic1 to Mic16) according to the recommendations of [6], whereas the red circles correspond to 5 equidistant microphones placed in a vertical plane in front of the antenna. Fig. 8 includes the comparison of the FRFs obtained from the model and experimental data, which are directly extracted from the system identification of the MIMO control test. The results on the left correspond to the sensor that achieves the lowest mean square error with respect to the test reference (Mic2), whereas the graph on the right shows the worst correlated results (Mic7). For this example only transfer functions with reference signal Drive1 were considered. On a first look, one can notice the good overall fit of the pressure levels computed by the Digital Twin, which, as described before, is only possible thanks to the introduction of all the transfer functions of the system in the simulation, as depicted in Section 3.

The FRF curves show clear interference patterns over the entire frequency range of study, which can be mainly attributed to interactions between the different loudspeaker radiations as well as standing waves appearing inside the test volume. Room modes can also contribute to the responses at the sensors below the Schroeder frequency [5], although these are not accounted in the current model which assumes free-field conditions beyond the stacks. One can also notice from the plots of the phase that the model accurately predicts the group delay of the signal, which is mainly caused by the latency introduced by the DSP and the cross-over filters described in Section 3.1.

A further evaluation of the model accuracy was performed by calculating the PSD values corresponding to a certain configuration of the input signals. For this purpose, uncorrelated sources are simulated via the following definition of the input SDM matrix in Eq. (17):

$$\boldsymbol{S}_{\boldsymbol{xx}}^{*} = \boldsymbol{I} \tag{18}$$

where $\boldsymbol{I}$ is the identity matrix of dimension 6×6. As a result, Fig. 9 includes the narrowband PSD at sensor Mic7 for both the simulated and experimental models, as well as the error between them. The graph shows that the numerical model captures fairly well the overall sound level, as both curves follow the same trend across the spectrum. However, local disparities are visible in the narrowband plot which are due to uncertainties in the model parameters. Indeed, these uncertainties cause the correlation error to be as high as 10 dB at a few spectral lines, although the mean value remains close to zero. To provide a more complete indicator of the validity of the proposed simulation models, Fig. 10(a) displays the spatial average of the SPL in one-third octave bands compared to the experimental one, showing that the average difference is kept under 3 dB in all bands. On the other hand, Fig. 10(b) shows the difference in the amplitude of the responses measured at each sensor analyzed in this exercise, which indicates that the modeling errors can increase locally at some sensors. It is pointed out that no detailed model update was performed to obtain these results. A deeper study on the model sensitivities may help improving further the correlation.

4.2. Error propagation

The uncertainties in the model parameters induce some errors in the simulation of the system responses which are reflected in the correlation of the FRF values, as shown in Fig. 8. In a MIMO system, these errors will propagate to the calculation of the SDM of

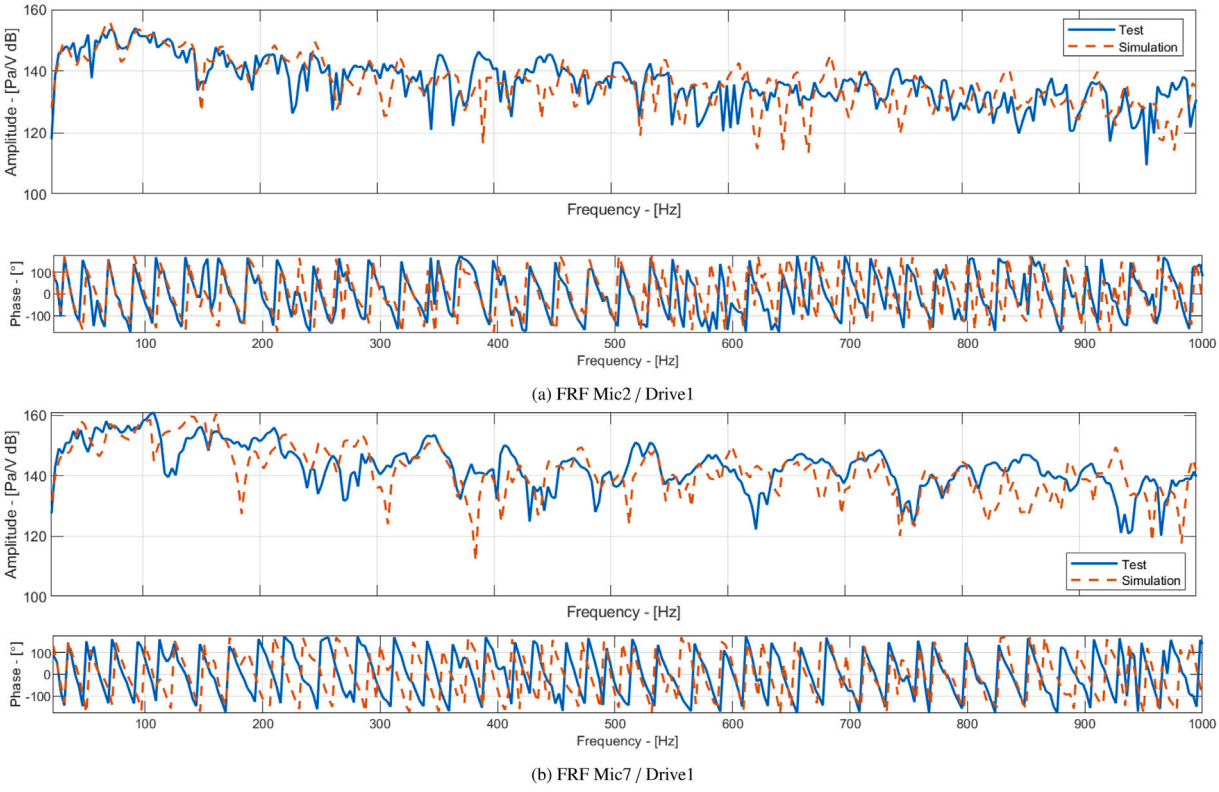

(a) FRF Mic2 / Drive1

(b) FRF Mic7 / Drive1

Fig. 8. Comparison between experimental and simulated FRF functions at the most (a) and least (b) accurate sensors.

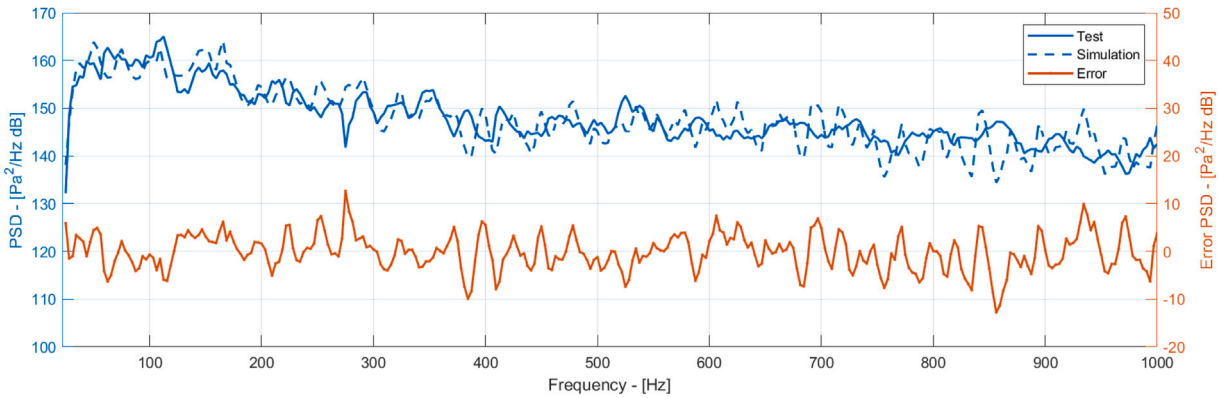

Fig. 9. Comparison of experimental and simulated PSD at sensor Mic7 with uncorrelated sources.

the responses via Eq. (17). This section provides some insights on how the modeling errors in the frequency response matrix might affect the accuracy of the PSD responses of the system. Because the model uncertainties are many and sometimes unknown, the current study applies a Monte-Carlo analysis to produce a distribution of spectral responses based on random errors applied directly at the components of the simulated FRF matrix. In this manner, a set of new matrices accounting for the imposed errors can be defined as

$$\boldsymbol{H}_{error} = \boldsymbol{E} \odot \boldsymbol{H}_{sim}, \tag{19}$$

where $\boldsymbol{E} \in \mathbb{C}^{n_m \times n_d}$ is the error matrix and $\odot$ refers to the Hadamard product, a.k.a. element-wise product. Owing to the definition of the acoustic references and tolerance limits in decibels in this kind of acoustic applications, the uncertainty is introduced accordingly, defined as a random deviation of the FRF values in $\boldsymbol{H}_{sim}$. Consequently, the real and imaginary components of $\boldsymbol{E}$ were defined

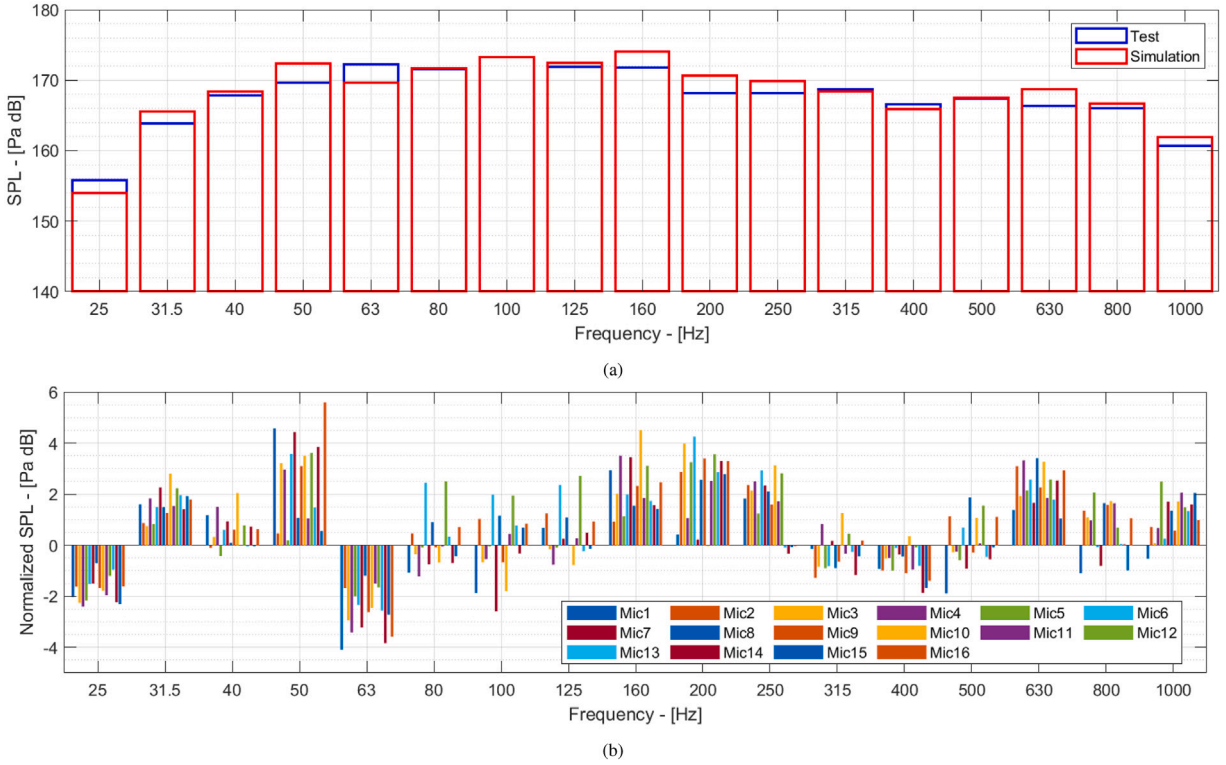

Fig. 10. Spatial average SPL of the experimental and simulated models (a) and amplitude difference at each microphone (b).

randomly from a normal distribution with a standard deviation equal to 3 dB from the original value of $\boldsymbol{H}_{\boldsymbol{sim}}$, as follows:

$$\boldsymbol{e}_{\boldsymbol{ij}} = 10^{\epsilon_{ij}/20} \tag{20}$$

with $\varepsilon_{ij} \sim \mathcal{N}(0, 3)$, being $\boldsymbol{e}_{\boldsymbol{ij}}$ the components of $\boldsymbol{E}$. Once a new frequency response matrix is computed, the synthesized PSDs are obtained by substituting $\boldsymbol{H}_{\boldsymbol{error}}$ in Eq. (17). A total of 10,000 iterations were performed to calculate a rich distribution of possible spectral responses. The two extreme scenarios of the MIMO problem were considered, i.e. uncorrelated sources and fully correlated sources. The former is obtained by defining the input SDM matrix as in Eq. (18), whereas the latter corresponds to a case in which

$$\boldsymbol{S}^{*}_{\boldsymbol{xx}} = \boldsymbol{J} \tag{21}$$

where $\boldsymbol{J} \in \mathbb{C}^{n_d \times n_d}$ is the all-ones matrix.

Fig. 11 shows the normal distribution parameters of the calculated PSD responses from the Monte Carlo analysis at sensor Mic7 for the uncorrelated (a) and fully correlated (b) signals. The plots include the mean PSD values as well as the standard deviation (in dB) of the aggregated results at each frequency line. For uncorrelated sources, the standard deviation in the responses is practically constant along the frequency axis and has a reduced average value (1.73 dB in Mic7) compared to that imposed in the input uncertainties (3 dB), meaning that random modeling errors in the simulated FRFs are contained. On the other hand, in the case of fully correlated sources, the distribution of acoustic responses varies along the frequencies and the standard deviation has a mean value which is slightly higher than 3 dB at all the considered microphones (4.10 dB in Mic7). Since, in a real control scenario, the SDM of the inputs will lie between these extreme cases, these findings suggest that the uncertainty of the synthesized spectral responses of the MIMO system is overall similar as that in the model of the transfer functions.

A further analysis was performed to study the effect that the modeling errors in the simulated FRFs have on the pre-test outcome, including the solution of the inverse problem to estimate the drive signals using Eq. (16) and the subsequent prediction of the pressure responses via Eq. (17). In this analysis, the reference SDM, $\boldsymbol{S}^{*}_{\boldsymbol{dd}}$, was generated from the same acoustic profile utilized in Section 4.3, and all 16 control candidates indicated in Section 4.1 are included in $\boldsymbol{H}^{\boldsymbol{c}}_{\boldsymbol{sim}}$. The result statistics are depicted in Fig. 12, including the predicted voltage signal of Drive1 (a) as well as the pressure response in Mic7 (b). The study shows that, for this realistic example, the estimated standard deviation in the voltage signals, $\boldsymbol{S}^{*}_{\boldsymbol{xx}}$, is contained, having a mean value of 2.21 dB over the analyzed frequencies. Subsequently, the resulting PSD of the estimated pressure shows that the dispersion of the error around the mean value is narrowed with respect to the imposed distribution in the FRF matrix, being the mean standard deviation equal to 1.31 dB. Similar values were obtained for the other drives and sensors. This remaining error propagating back to the pressure responses after the full pre-test operations can be explained by the approximated solution of the overdetermined ($n_m > n_d$) inverse

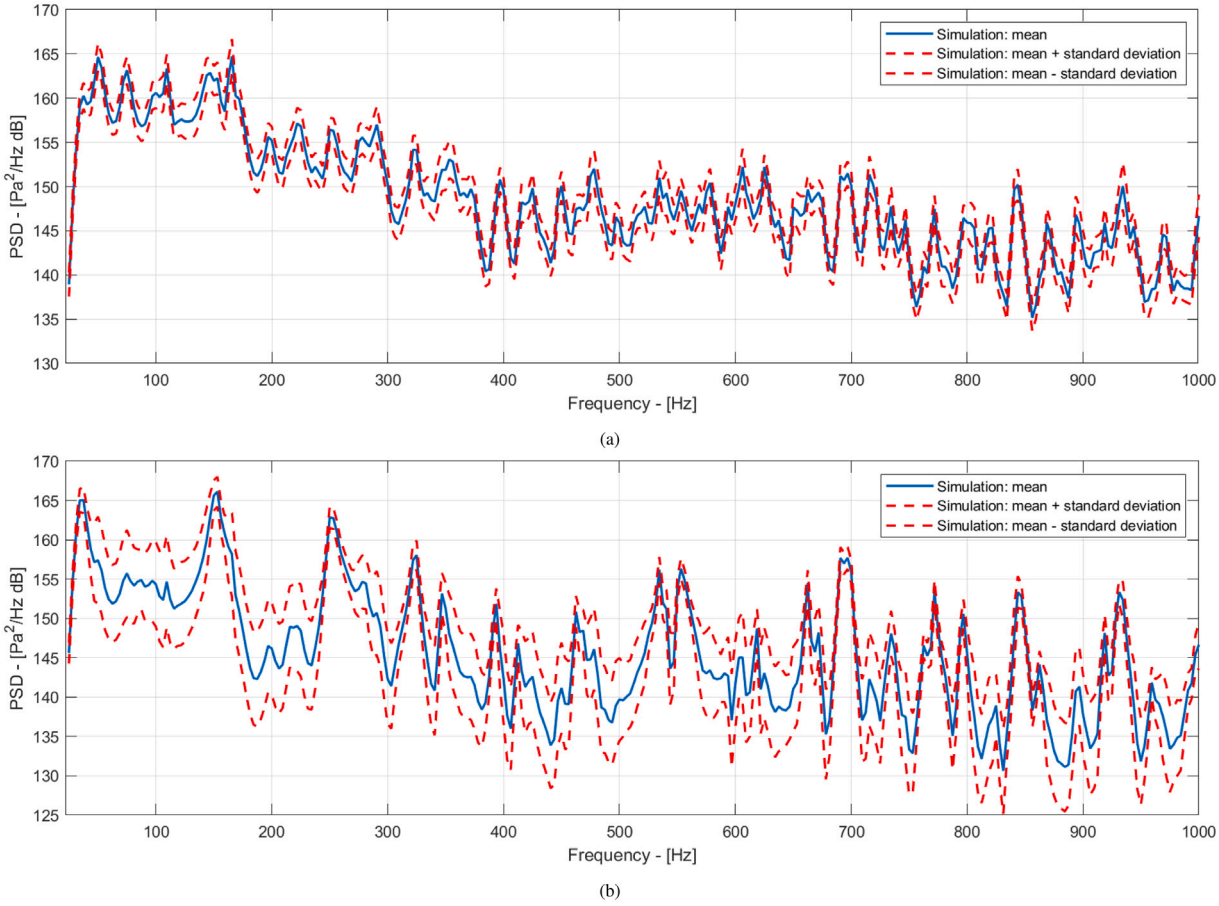

Fig. 11. Error propagation in the feedforward MIMO problem based on a Monte-Carlo analysis: mean and standard deviations of the PSD at Mic7 for uncorrelated (a) and fully correlated (b) sources.

problem. Indeed, the solution of a square problem ($n_m = n_d$) leads to a zero standard deviation after performing Eqs. (16) and (17). The generalization of these findings to other cases depends on the type and location of the random errors, as well as on how well-conditioned the MIMO problem is, which is defined by the properties of $\boldsymbol{H}^{\boldsymbol{c}}_{\boldsymbol{sim}}$.

4.3. Pre-test validation

Subsequently, the validity of the proposed Digital Twin to perform virtual pre-test analyses is demonstrated via direct comparison against the experimental solutions. To do this, first a pre-test analysis was conducted using the simulated transfer functions of the 16 sensors shown in yellow in Fig. 7(a). The following parameters were defined:

- number of microphones selected for control = 12
- number of iterations to improve target realizability via UPA = 1200
- number of candidates for the optimal sensor selection = 1820 (maximum number of possible combinations without repetition)

The acoustic reference profile used for the pre-test was that employed in the DFAX test (138 dB) performed in 2017. The resulting metrics of the optimization algorithm are included in Fig. 13, which shows the number of bands exceeding the tolerance limits in increasing order (a) as well as the RMSE of each control candidate (b). As described in [8], the selection of control sensors is critical to avoid suboptimal candidates, which may lead to control instabilities due to conditioning issues [24]. Based on these results, the candidate with the least number of bands out of tolerance was chosen to simulate the frequency responses of the system.

To obtain the experimental references, the pre-test analysis was repeated but this time using the transfer functions from the experimental test. To allow for a direct comparison of the results, the set of control sensors was fixed to the outcome of the previous virtual pre-test. Fig. 14 includes the SPL values in one-third octaves normalized with respect to the reference values for the experimental model (a) and the numerical one (b). The results display the dispersion of all 16 sensors (control and monitoring) with respect to the target profile, as well as the spatial average. The tolerance (Up/Low alarm) and abort (Abort level) bands defined in

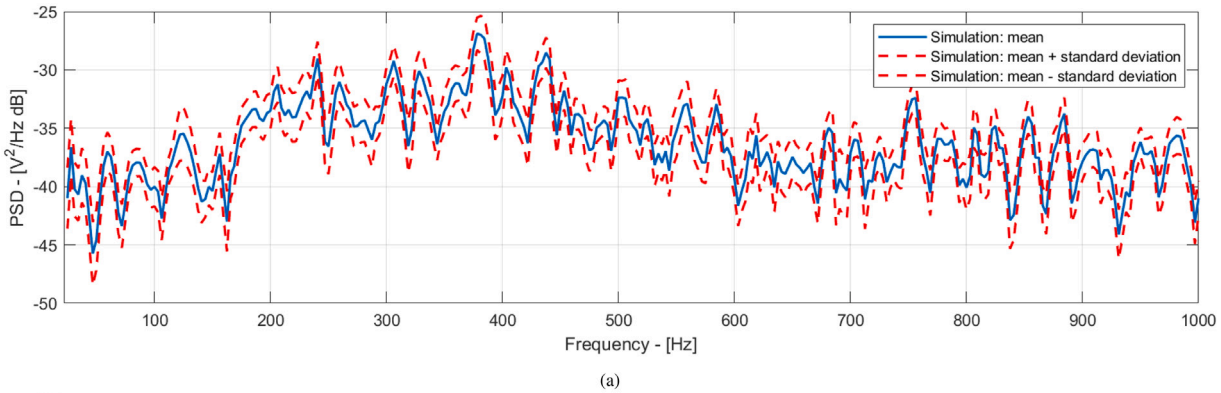

(a)

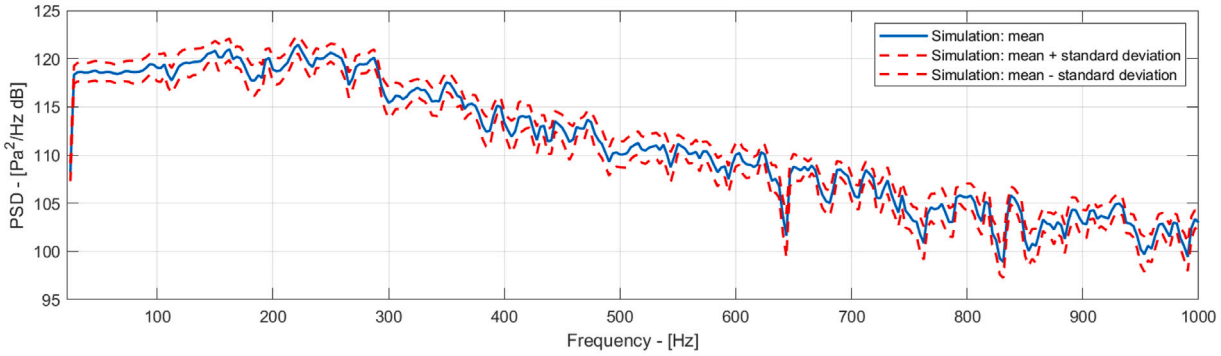

(b)

Fig. 12. Error propagation in the full pre-test analysis: mean and standard deviations of the PSD of the voltage signal at Drive1 (a) and of the estimated pressure at Mic7 (b).

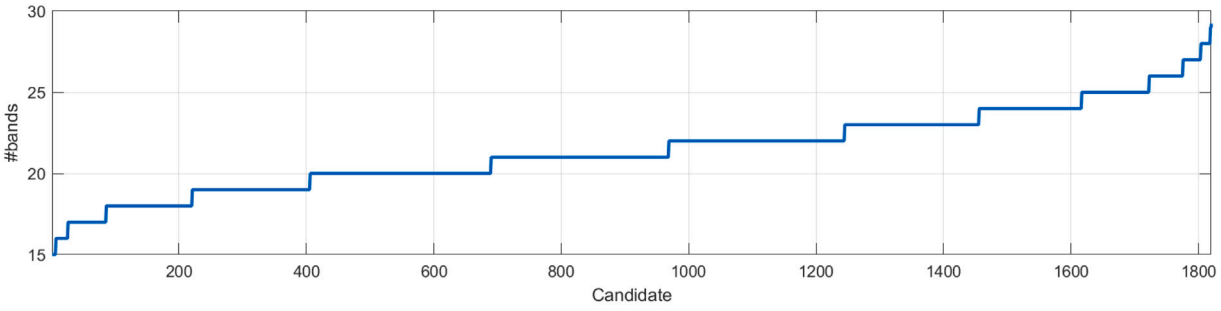

(a)

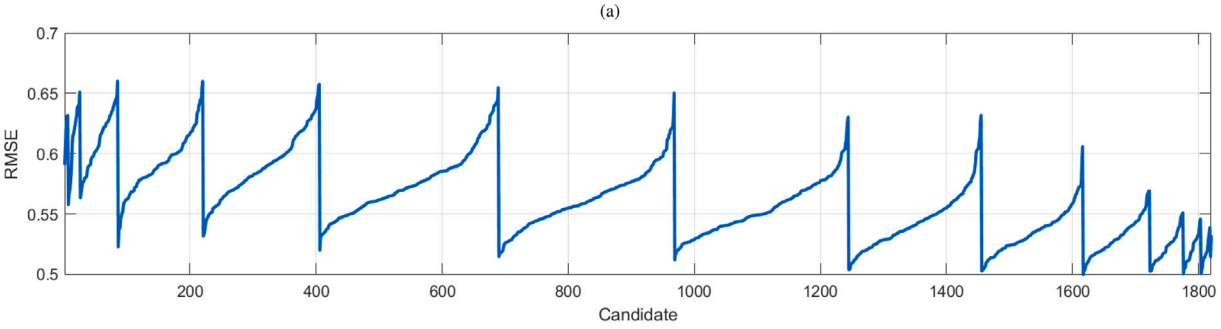

(b)

Fig. 13. Pre-test metrics including (a) number of bands out of tolerance and (b) RMSE.

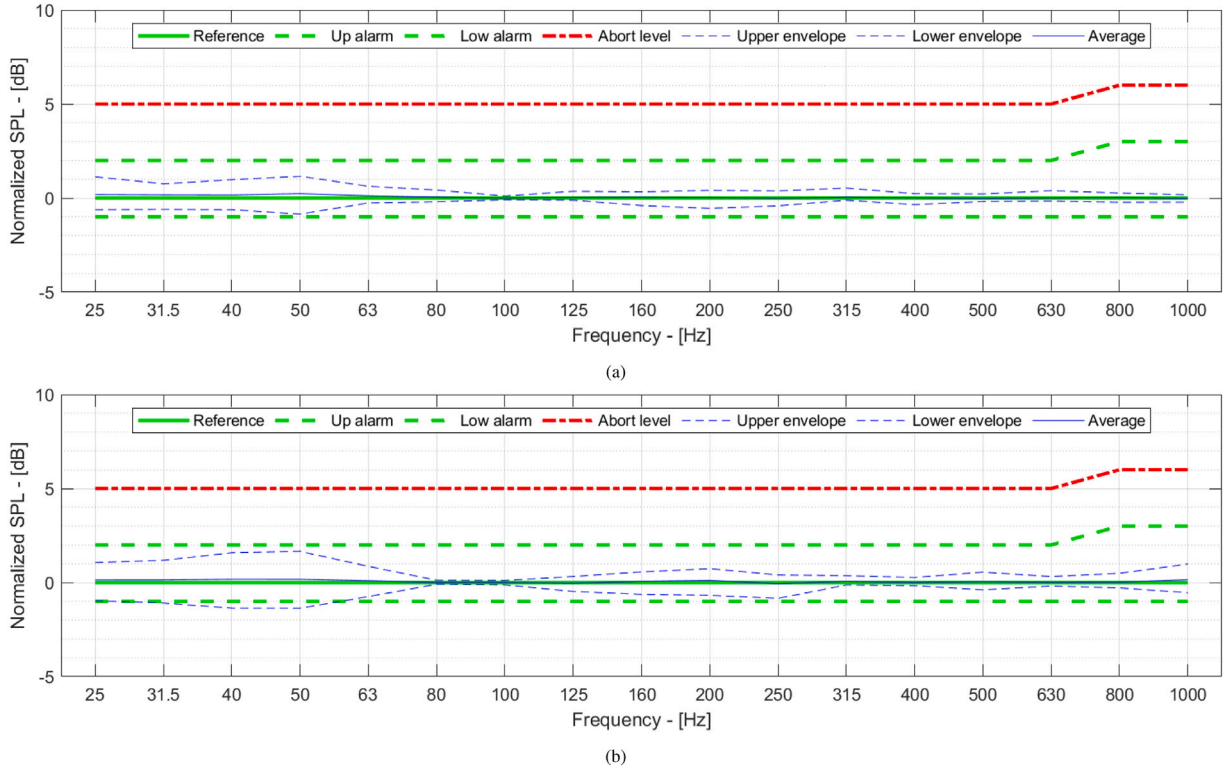

Fig. 14. Normalized SPL with respect to the one-third octave reference profile: (a) experimental pre-test and (b) virtual pre-test.

the test are added as well for reference purposes. It is possible to observe that the predicted acoustic responses are quite similar in both models, specially in terms of the response average. A slightly higher dispersion is visible in the simulated sensors, mainly at the low frequency bands. Indeed, a few bands computed by the virtual model fall below the lower tolerance (−1 dB), whereas in the experimental model the envelope of the acoustic responses remains within tolerance. However, in view of the overall results, the accuracy of the virtual pre-test for the electro-acoustic plant under study was satisfactory.

The main goal of environmental acoustic tests is to recreate the diffuse sound field that is assumed inside the fairing during launch. Ideally, this means that the acoustic level should be the same at all locations, and that the spatial correlation between linear quantities measured at two points only depend on the distance between them. A model of the spatial coherence between two sensors placed in a reverberant room is provided by the following formula [4]:

$$\gamma^2(\omega, r) = \left(\frac{sin(\omega r/c)}{\omega r/c} \right)^2, \tag{22}$$

where ω is the angular frequency, c is the speed of sound and r is the distance between the sensors. This analytical model is here used as a reference to evaluate the sound diffuseness obtained from the spectral responses synthesized from the experimental and numerical models. For the latter models, the average coherence was computed directly from the output responses using the following formula [2]:

$$\gamma^2_{ab} = \frac{|\langle S_{ab} \rangle|^2}{\langle S_{aa} \rangle \langle S_{bb} \rangle}, \tag{23}$$

where a and b are the sensor indexes. The 5 microphones marked in red in Fig. 7(a) are used for the calculations, as they include 4 pairs of sensors disposed in a vertical plane and featuring the same distance. The results are displayed in Fig. 15. One can observe that beyond 150 Hz, approx., the sound field in the vertical is not perfectly diffuse, which agrees well with past studies on environmental acoustic tests, see for instance [38]. It is remarked that the aim of the current analysis is not to discuss the spatial coherence of the acoustic responses in the test, but to demonstrate that the behavior of the coherence predicted by the simulation matches fairly well that from the experimental references in DFAX.

4.4. Virtual pre-test results

After assessing the use of the virtual pre-test analysis for the accurate simulation of the MIMO control responses, the final analysis focuses on the potential of full-field data for improving the control strategy before the test campaign takes place. For that end, the

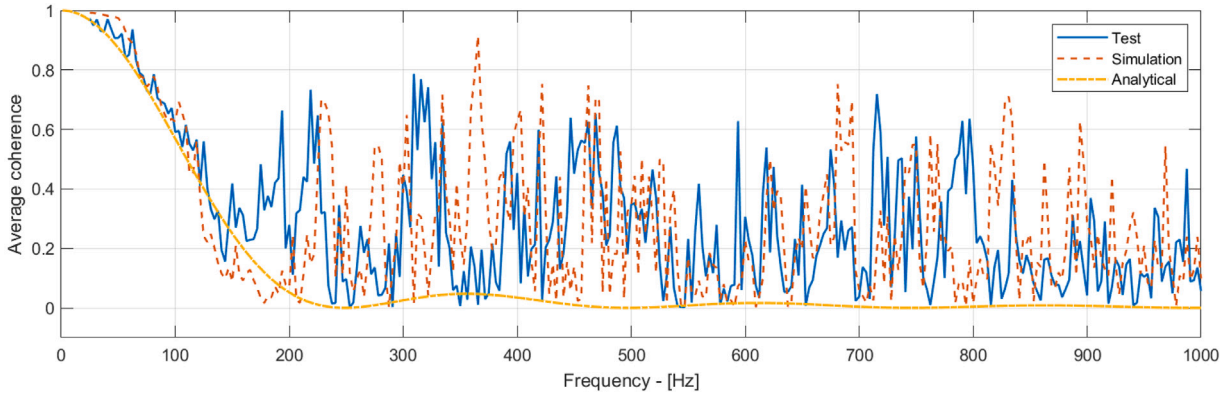

Fig. 15. Average spatial coherence computed using the responses at 5 sensors located in a vertical plane.

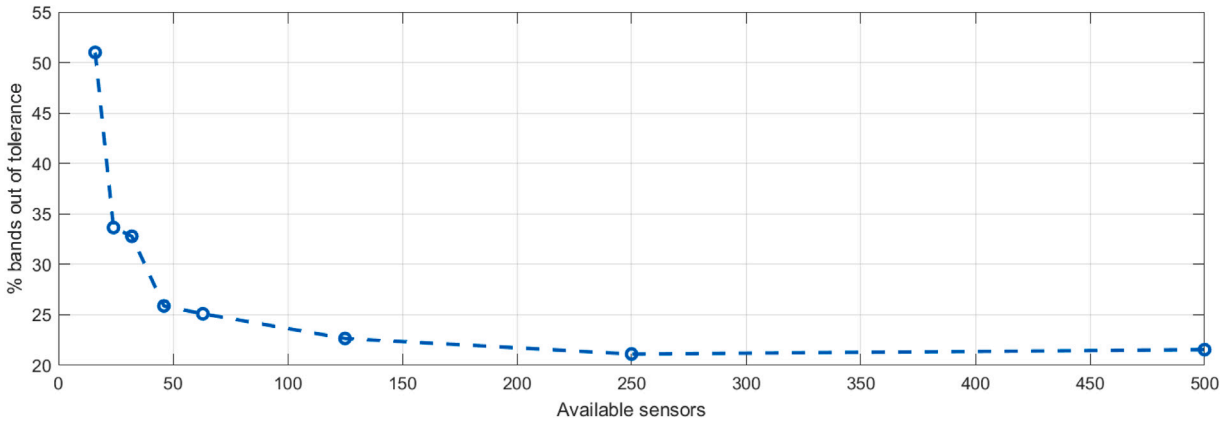

Fig. 16. Percentage of bands out of tolerance for an increasing number of available sensors in the virtual test. The number of sensors utilized in each pre-test analysis is 16, 24, 32, 46, 63, 125, 250 and 500.

pre-test analysis is performed making use of the acoustic responses at a dense set of virtual sensors located around the test specimen. The goal is to perform a better selection of control sensors by discarding more sub-optimal candidates based on a much larger space of potential responses.

In this exercise, a total of 500 microphones were generated around the test specimen, randomly located over a hollowed cylindrical volume outer radius equal to 1.715 m and inner radius equal to 1.2 m and spanning from 0.5 to 3.5 m of distance to the ground. Fig. 7(b) displays the model with all the sensors included in the analysis. A series of virtual pre-test analyses were performed using subsets of the available sensors as candidates for control, starting from $T = 16$ sensors up to $T = 500$. The same parameters as in the previous example were defined, i.e. 12 control sensors, 1200 projection iterations and 1820 combinations for the candidate optimization. For each pre-test run, the metrics of the best candidate are stored and compared. Fig. 16 shows the percentage of bands out of tolerance found for all the pre-test runs. The asymptotic trend of the graph indicates that there is a minimum number of candidate sensors that allows the pre-test algorithm to map the acoustic field with an acceptable degree of accuracy in the range of frequencies targeted in the study. Based on this analysis, the test designer has at hand an indicator of the trade off between the number of sensors to be installed and the performance in terms of sound level uniformity in the control volume.

Another implication of the results included in Fig. 16 is that there seems to be a ceiling on the pressure uniformity that can be reached for a given configuration of the control system. Indeed, in spite of the amount of sensors utilized in the pre-test analysis, the number of bands out of tolerance remains in all cases above 20% in this exercise. It is however pointed out that many other parameters play a role in the capability of the DFAX plant to achieve the desired levels of field uniformity, such as the number of control sensors (here fixed as 12) and the disposition of the drive signals in the electro-dynamic transducers, among others. Although analyzing the sensitivity of the field uniformity against all these aspects is definitely of great interest, it remains out of the scope of the present work. Looking only at the number of available sensors for pre-test, the gain in sound uniformity is further proven in Fig. 17, which displays the SPL octave values normalized with the reference profile at all 500 sensors for two of the pre-test runs, those utilizing 16 and 125 sensors for control, respectively. The blue lines correspond to the average SPL values and the maximum and minimum deviation, normalized with respect to the test reference. One can observe that both the dynamic range as well as the average pressure level are improved considerably by adding field points in the control volume.

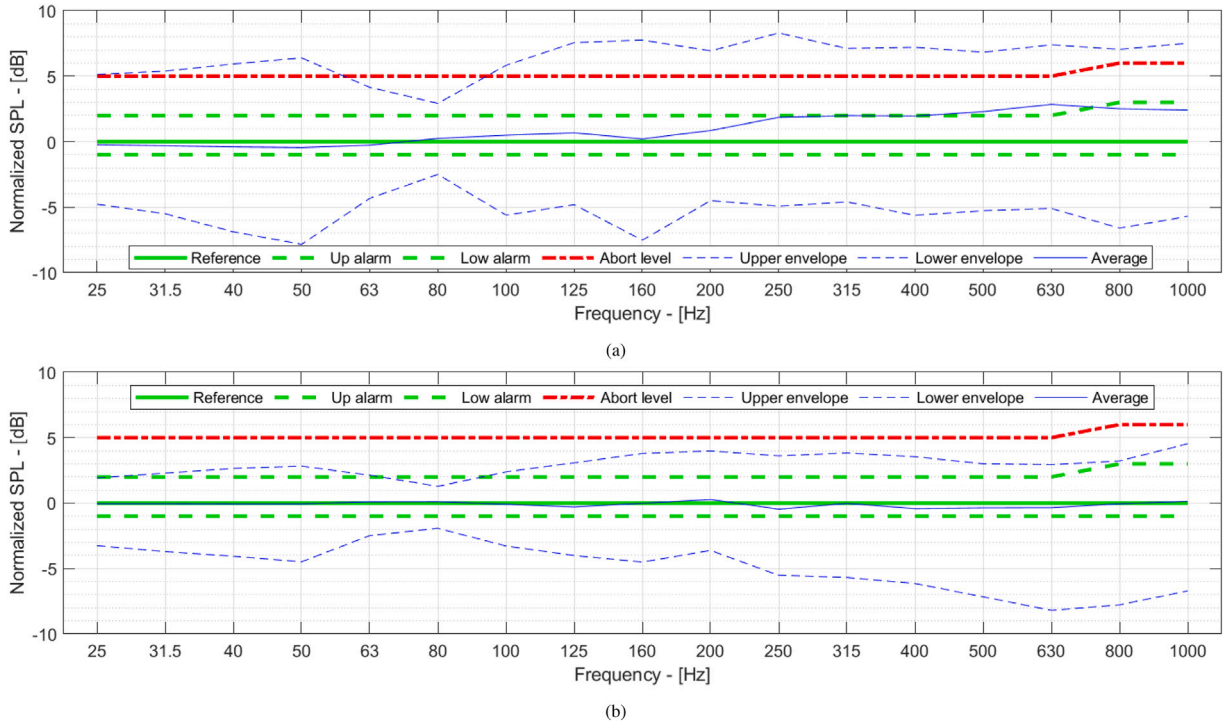

Fig. 17. Normalized SPL with respect to the one-third octave test references. The results correspond to the pre-tests based on 16 sensors (a) and 125 sensors (b).

The data acquired from the Digital Twin can be used by test engineers to gain more useful insight of the control system performance and the achieved pressure fields around the test specimen [16,17]. An example of this capability in the Simcenter 3D environment is illustrated in Fig. 18, which show the SPL fields at the 125 and 800 one-third octave bands obtained from the virtual pre-test analysis. Such contour plots can provide crucial information of the acoustic (and structural) responses that can be expected during the physical test at all locations. The full-field solutions have the ability to point out any potential risk of the chosen control strategy so that corrective actions can be taken already at an early stage in the test preparation, avoiding time and cost consuming changes on-site during the actual test. As an example, for the studied MIMO control system the plots in Fig. 18 show that although within the control volume the SPL range remains acceptable, high pressure zones appear in the center of the test volume at certain bands. This effect can be explained by various reasons: first, the lack of sensors allocated in this exercise to the center region is preventing the control strategy to have any effect in that area, thus standing waves in between the stacks are not fully controlled. This phenomena is indeed evident at low/mid frequencies where the acoustic wavelengths are of the same order of magnitude as the radius of the set up, as it is shown in Fig. 18(a). Secondly, vibro-acoustic interaction with the structure under test generates high pressure areas on the antenna's surface, as it is observed in Fig. 18(b). This type of acoustic responses can only be captured via full-field monitoring of the DFAX system. Although in this work the Digital Twin is used as a tool for the test design, further extensions of the same modeling approach could be used for on-line monitoring and enhanced post-processing of the test data via virtual sensing strategies [39,40].

5. Summary and conclusions

The present paper presents a Digital Twin for the prediction of the responses of multi-channel control strategies in direct field acoustic excitation tests (DFAX). The analysis includes a comprehensive modeling procedure for the prediction of the frequency responses of the electro-acoustic plant as well as the behavior of the multiple-input multiple-output (MIMO) random control system. The proposed virtual approach can be employed to improve the design of the test configuration, with particular emphasis on the control parameters. With that purpose in mind, inspired by the experimental pre-test analysis, a procedure to optimize the location of the control sensors based on simulated data is implemented and validated. Such approach has the potential to reduce the duration and risks of the test campaign by allowing test engineers to make informed decisions at an early stage.

In order to predict the electro-acoustic behavior of the test plant with a sufficient degree of accuracy, all the signal transformations (power amplification, loudspeaker response, acoustic propagation and vibro-acoustic couplings with test specimen) are accounted for in the Digital Twin. Such modeling approach leads to the prediction of the transfer functions of the full system, from the signal generator to the field sensors. The availability of this data is paramount if one desires to replicate the behavior of MIMO strategies

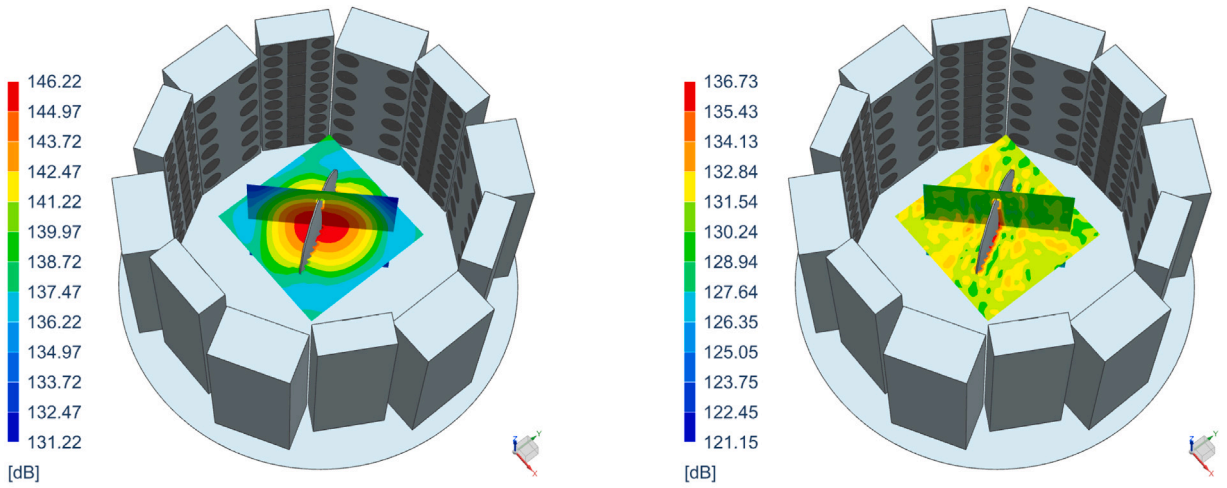

(a) 125 Hz (b) 800 Hz

Fig. 18. Contour plots of the SPL over two microphone planes at two one-third octave bands.

for different configurations of the control settings. In addition, numerical models generate full-field data over the acoustic volume and structural specimen, thus providing a more complete insight of the DFAX responses as compared to the actual test where only a few sensors are available.

The accuracy levels achieved by the simulation are assessed via comparison against experimental references from a DFAX test campaign conducted a few years prior to the present work. The results show that the model is able to predict the acoustic responses at the microphone sensors with enough precision to be used for design purposes and parameter tuning. To demonstrate that, the outcome of the virtual pre-test analysis is displayed together with that from experimental data, proving the ability of the Digital Twin to simulate similar values of sound pressure level and spatial correlation.

The availability of unlimited virtual sensors has the potential to extend the ability of the MIMO controller to better reproduce the expected uniform sound fields. Furthermore, full-field solutions can help de-risking the test by identifying critical areas that might be overlooked with a finite number of sensors. Although in this work the virtual pre-test addresses mainly the automatic selection of the control microphones for a given electro-acoustic setup, an extension of the current approach for the optimization of other control parameters such as the control volume, drive matrix, specimen orientation and geometrical layout, among others, would be straightforward. Future research activities will also focus on the sensitivity of the structure response with respect to the test configuration and control strategy, which is considered of major interest by the acoustic testing community.

The proposed modeling framework can be used to predict the MIMO system responses before the physical set-up is installed based on known inputs and model parameter estimations. To complete the Digital Twin for environmental acoustic tests, the capability of correlating and updating the model onsite once the test is being conducted must be included. Such set of tools, which will enable the mitigation of the model uncertainties, is currently under development and will be discussed in future works.

Declaration of competing interest

The authors declare that they have no known competing financial interests or personal relationships that could have appeared to influence the work reported in this paper.

Data availability

The authors do not have permission to share data.

Acknowledgments

The authors gratefully acknowledge the Belgian Federal Science Policy Office (BELSPO) and the European Space Agency (ESA) for their support through the General Support Technology Programme (No. 4000127640/19/NL/GLC/vr). The authors would like to also thank Thales Alenia Space for its collaboration in the testing activities and for providing the structural model of the test specimen.

References

[1] NASA-HDBK-7008 Spacecraft Dynamic Environments Testing, Technical report, NASA, 2016.
[2] F. Jacobsen, T. Roisin, The coherence of reverberant sound fields, J. Acoust. Soc. Am. 108 (1) (2000) 204–210.
[3] ECSS-E-HB-32-26A Spacecraft Mechanical Loads Analysis Handbook, Technical report, European Cooperation for Space Standarization, 2013.
[4] R.K. Cook, R.V. Waterhouse, R.D. Berendt, S. Edelman, M.C. Thompson, Measurement of correlation coefficients in reverberant sound fields, J. Acoust. Soc. Am. 27 (6) (1955) 1072–1077.
[5] M. Schroeder, K. Kuttruff, On frequency response curves in rooms. Comparison of experimental, theoretical, and Monte Carlo results for the average frequency spacing between maxima, J. Acoust. Soc. Am. (1962).
[6] NASA-HDBK-7010 Direc Field Acoustic Testing (DFAT), Technical report, NASA, 2016.
[7] P.A. Larkin, Developments in direct-field acoustic testing, Sound Vib. 48 (2014) 6–10.
[8] M. Alvarez Blanco, P. Van Vlierberghe, M. Rossetti, K. Janssens, B. Peeters, W. Desmet, Pre-test analysis to reproduce random pressure fields with multi-channel acoustic control, Mech. Syst. Signal Process. 163 (2022) 108103.
[9] M. Alvarez Blanco, G. Bitetti, U. Musella, A. Ciriello, V. Di Pietro, B. Peeters, Direct field acoustic test of European space hardware at system level of assembly, in: Proceedings of 16th European Conference on Spacecraft Structures, Materials and Environmental Testing, 2021.
[10] M.G. Ostergaard, A.R. Ibbotson, O.L. Roux, A.M. Prior, Virtual testing of aircraft structures, CEAS Aeronaut. J. 1 (2011).
[11] S.-H. Xianga, C. Liu, T. Yan, Virtual vibration test and verification for the satellite, in: Proceedings of the 14th International Congress on Sound and Vibration, 2007.
[12] F. Huizinga, R.A.A.V. Ostaijen, A. Van Oosten Slingeland, A practical approach to virtual testing in automotive engineering, J. Eng. Des. 13 (2002) 33–47.
[13] M. Remedia, G.S. Aglietti, M. Appolloni, A. Cozzani, A. Kiley, An enhanced methodology for spacecraft correlation activity using virtual testing tools, J. Sound Vib. 409 (2017) 180–200.
[14] G.S. Aglietti, M. Remedia, M. Appolloni, A. Kiley, Spacecraft structure model validation and test philosophy, AIAA J. 57 (5) (2019) 2109–2122.
[15] S. Ricci, B. Peeters, J. Debille, L. Britte, E. Faignet, Virtual shaker testing: a novel approach for improving vibration test performance, in: Proceedings of the 2008 International Seminar on Modal Analysis, 2008.
[16] M. Alvarez Blanco, E. Matas, H. Bériot, B. Peeters, W. Desmet, Frequency dependent selection of control sensors in multi-channel acoustic control, CEAS Space J. 13 (2021) 119–131.
[17] M. Alvarez Blanco, Pre-test Analysis for Multi-Channel Acoustic Control (Ph.D. thesis), Katholieke Universiteit Leuven, 2021.
[18] M. Alvarez Blanco, R. Hallez, K. Janssens, F. Bianciardi, A. Carrella, Simulation and validation of a MIMO direct field acoustic control system for acoustic qualification tests, in: Proceedings of 30th Aerospace Testing Seminar, 2017.
[19] A.G. de Miguel, M. Alvarez Blanco, E. Matas, H. Bériot, J. Cuenca, I.C.S. Ngan, B. Peeters, Numerical pre-test analysis for multi-channel control strategies in environmental acoustic tests, in: Proceedings of 16th European Conference on Spacecraft Structures, Materials and Environmental Testing, 2021.
[20] L.L. Beranek, T.J. Mellow, Acoustics: Sound Fields and Transducers, Academic Press, Oxford, 2012.
[21] H. Bériot, A. Prinn, G. Gabard, Efficient implementation of high-order finite elements for Helmholtz problems, Internat. J. Numer. Methods Engrg. 106 (3) (2016) 213–240.
[22] H. Bériot, A. Modave, An automatic perfectly matched layer for acoustic finite element simulations in convex domains of general shape, Internat. J. Numer. Methods Engrg. 122 (5) (2021) 1239–1261.
[23] ECSS-E-ST-10-03C – Testing, Technical report, European Cooperation for Space Standarization, 2012.
[24] S.J. Elliott, Signal Processing for Active Control, Elsevier, 2000.
[25] G. Golub, C. van Loan, Matrix Computations, third ed., The Johns Hopkins University Press, London, 1996.
[26] G.P. Geaves, D.J. Henwood, Finite element modelling of a loudspeaker. Part 1: theory and validation, J. Audio Eng. Soc. (2005).
[27] R. Lerch, M. Kaltenbacher, M. Meiler, Virtual prototyping of electrodynamic loudspeakers by utilizing a finite element method, J. Acoust. Soc. Am. 123 (5) (2008) 3643.
[28] M. Karjalainen, V. Ikonen, P. Antsalo, P. Maijala, L. Savioja, A. Suutala, S. Pohjolainen, Comparison of numerical simulation models and measured low-frequency behavior of loudspeaker enclosures, J. Audio Eng. Soc. 49 (12) (2001) 1148–1166.
[29] Y. Shiozawa, R. d'Amico, H. Onitsuka, W. Desmet, A multi-physical loudspeaker model including experimental modal information of the membrane, in: Proceedings of ISMA2014, 2014.
[30] N. Thiele, Loudspeakers in vented boxes: part 1, J. Audio Eng. Soc. 19 (5) (1971) 382–392.
[31] R.H. Small, Vented-box loudspeaker systems–part 1: small-signal analysis, J. Audio Eng. Soc. 21 (5) (1973) 363–372.
[32] W. Klippel, Tutorial: loudspeaker nonlinearities — causes, parameters, symptoms, J. Audio Eng. Soc. 54 (10) (2006) 907–939.
[33] A. Lieu, G. Gabard, H. Bériot, A comparison of high-order polynomial and wave-based methods for Helmholtz problems, J. Comput. Phys. 321 (2016) 105–125.
[34] B. Gilvey, J. Trevelyan, A comparison of high-order and plane wave enriched boundary element basis functions for Helmholtz problems, Eng. Anal. Bound. Elem. 122 (2021) 190–201.
[35] H. Bériot, G. Gabard, Anisotropic adaptivity of the p-FEM for time-harmonic acoustic wave propagation, J. Comput. Phys. 378 (2019) 234–256.
[36] C.B. Barber, D.P. Dobkin, H. Huhdanpaa, The quickhull algorithm for convex hulls, ACM Trans. Math. Softw. 22 (4) (1996) 469–483.
[37] P.R. Amestoy, I.S. Duff, J. Koster, J.-Y. L'Excellent, A fully asynchronous multifrontal solver using distributed dynamic scheduling, SIAM J. Matrix Anal. Appl. 23 (1) (2001) 15–41.
[38] C. Fabries, B. Brevart, A. Carrella, M. Alvarez Blanco, D. Dal Fitto, S. Charfenberg, Experimental validation of direct field acoustic testing, in: Proceedings of 14th European Conference on Spacecraft Structures, Materials and Environmental Testing, 2016.
[39] A. van de Walle, F. Naets, W. Desmet, Virtual microphone sensing through vibro-acoustic modelling and Kalman filtering, Mech. Syst. Signal Process. 104 (2018) 120–133.
[40] H. Van der Auweraer, T. Tamarozzi, E. Risaliti, M. Sarrazin, J. Croes, B. Forrier, F. Naets, W. Desmet, Virtual sensing based on design engineering simulation models, in: ICEDyn2017 International Conference on Structural Engineering Dynamics, 2017.